Supramolecular Chemistry
Publication details, including instructions for authors and subscription information:
http://www.informaworld.com/smpp/title~content=t713649759

Cholic Acid Inclusion Compounds with Aromatic Guests: Structures and Decomposition Kinetics

Janet L. Scott[a]
[a] Department of Chemistry, University of Cape Town, Rondebosch, South Africa

To cite this Article Scott, Janet L.(1997) 'Cholic Acid Inclusion Compounds with Aromatic Guests: Structures and Decomposition Kinetics', Supramolecular Chemistry, 8: 3, 241 — 248
To link to this Article: DOI: 10.1080/10610279708034941
URL: http://dx.doi.org/10.1080/10610279708034941

SUPRAMOLECULAR CHEMISTRY, 1997, Vol. 8, pp. 241–251
Reprints available directly from the publisher
Photocopying permitted by license only

Cholic Acid Inclusion Compounds With Aromatic Guests: Structures and Decomposition Kinetics

JANET L. SCOTT

Department of Chemistry, University of Cape Town, Rondebosch, 7700, South Africa

(Received 11 December 1996)

Cholic acid forms 1:1 (host:guest) inclusion compounds with a variety of aromatic guest molecules. The crystal structures of the inclusion compounds with benzonitrile and *p*-nitro toluene have been elucidated. CA·benzonitrile: space group $p2_1$, a = 13.642(3), b = 8.133(2), c = 14.055(3) Å, β = 114.12(2)°, Z = 2, D_c = 1.194 g.cm^{-3}, final R factor = 0.0781 for 1853 independent reflections. CA·*p*-nitro toluene: space group $P2_1$, a = 13.495(1), b = 8.266(4), c = 14.398(2) Å, β = 114.61(1)°, Z = 2, D_c = 1.249 g.cm^{-3}, final R factor = 0.0608 for 2783 independent reflections. The kinetics of decomposition of these and related compounds are investigated and kinetic parameters *Ea* and *In A* so derived compared and contrasted.

3α, 7α, 12α-trihydroxy-5β-cholan-24-oic acid or Cholic acid (CA) has been shown to form inclusion compounds with a variety of guest molecules. The 1:1 inclusion compounds with methanol, ethanol and *n*-propanol[1,2,3] exhibit extensive host-host and host-guest hydrogen bonding and the guest molecules are accommodated in cavities. The structures of the hydrate[4] and hemihydrate[5,6] are composed of hydrogen-bonded bilayers and helical columns respectively while the inclusion compound with acetone and three water molecules[7] is composed of bilayers of host and guest hydrogen bonded together in a system containing ten unique hydrogen bonds.

The bulk of CA inclusion compounds crystallise as tubulate clathrates in which host molecules are hydrogen bonded together in a head to tail fashion to form puckered bilayers with the hydrophobic β faces exposed on the bilayer surfaces. These bilayers are in turn packed such that channels remain between them in which guest molecules are stacked in columns parallel to the *b* crystallographic direction. Guest molecules such as aliphatic ketones[8], lactones[9], aliphatic[10] and vinyl esters as well as the aromatic guests nitrobenzene, aniline[11], acetophenone[12] and benzene[13] are included in this manner.

Given the similarities in the structures of these compounds we decided to investigate the kinetics of decomposition with the aim of relating reactivity to structure at a molecular level. The kinetics of decomposition of a variety of inorganic salts and hydrates have been extensively studied[14,15,16] and the effects of changes in reaction conditions, particle size and sample pretreatment investigated.[17,18,19] The decomposition kinetics of solid organic clathrates has not been considered in spite of the potential insights into stability and host-guest interactions to be gained therefrom.

We present the decomposition kinetics of a group of CA inclusion compounds with the aromatic guest molecules benzonitrile (CABN), aniline (CAAN), nitrobenzene (CANI), *p*-nitro-toluene (CAPNOT) and *p*-toluidine (CAPTOL). Possible mechanisms for the decomposition reaction are advanced and the crystal structures of CA with benzonitrile and *p*-nitro-toluene guests are presented while those of the other inclusion compounds included in this study have been published elsewhere.[11,20]

EXPERIMENTAL

Single crystals of the inclusion compounds were grown by slow evaporation of solutions of dry CA and the guest species dissolved in dry ace-

tone. The crystals grew as colourless needles in each case and suitable fragments for single crystal X-ray diffractometry were cut from these. The crystals were sealed in Lindemann capillary tubes with mother liquour as, although all of the compounds studied were stable in air at ambient temperatures for periods far exceeding that required for data collection, the crystals of the inclusion compounds of CA are often attacked by vapours of the materials used to secure crystals to glass fibres. Preliminary cell parameters were obtained photographically and intensity data were collected on an Enraf-Nonius CAD4 diffractometer at 294 K using graphite monochromated Mo-K_α radiation (λ = 0.7107 Å) and the ω–2θ scan mode. During data collection three reference reflections were monitored periodically to check crystal stability. The data were corrected for Lorentz-polarisation effects. Refined unit cell parameters were obtained by least-squares analysis of 24 reflections measured on the diffractometer in the range $16 < \theta < 17°$. Crystal data and other experimental details are given in Table I.

Structure Solution and Refinement

Both inclusion compound structures were solved by direct methods using the program SHELXS-86[21] and refined by full-matrix least-squares refinement using the program SHELX-76[22], refining on F, in the case of CABN and SHELXL-93[23], refining on F^2, in the case of CAP-

TABLE I Crystal data, experimental and refinement parameters.

	CABN	CAPNOT
Crystal Data		
Guest	Benzonitrile	*p*-Nitrotoluene
Molecular formula	$C_{24}H_{40}O_5$ ·C_7H_5N	$C_{24}H_{40}O_5$ ·$C_7H_7NO_2$
Molecular weight ($gmol^{-1}$)	511.703	545.717
Space Group	$P2_1$	$P2_1$
a(Å)	13.642(3)	13.495(1)
b(Å)	8.133(2)	8.266(4)
c(Å)	14.055(3)	14.398(2)
α(°)	90.0	90.0
β(°)	114.12(2)	114.61(1)
γ(°)	90.0	90.0
V(Å^3)	1423.3(6)	1451.1(7)
Z	2	2
D_c(gcm^{-3})	1.194	1.249
D_m(gcm^{-3})	1.189(3)	1.213(4)
μ(MoKα) (cm^{-1})	0.74	0.81
F(000)	556	592
Data collection		
Crystal dimensions (mm)	0.35 × 0.3 × 0.35	0.2 × 0.2 × 0.25
Range h, k, l	±16, 9, 16	16, 9, ±16
Total exposure time (h)	23.3	22.4
Intensity variation (%)	−9.7	1.7
No. of reflections collected	2821	2860
Final refinement		
No. of reflections (independent)	1853	2738
No. of parameters	306	364
$\Delta\rho_{max}$ ($eÅ^{-3}$)	0.31	0.36
$\Delta\rho_{min}$ ($eÅ^{-3}$)	−0.16	−0.36

NOT. The weighting scheme employed for CABN was $w = [\sigma^2(F) + 0.0075F_o^2]^{-1}$ chosen to ensure constant distribution of $<w(|F_o| - |F_c|)^2>$ with respect to sin θ and $(F_o/F_{max})^{1/2}$ and final R factors were: R = 0.0781 and wR = 0.0876 with S = 1.59. The weighting scheme employed for CAPNOT was $w = [\sigma^2(F_o^2) + (0.0955P)^2 + 0.1906P]^{-1}$, where $P = [Max(0,F_o^2) + 2F_c^2]/3$ and the final R factors were: $R_1 = 0.0608$ and $wR_2 = 0.1489$ for $1 > 2\sigma(I)$; $R_1 = 0.1714$, $wR_2 = 0.1882$ for all data with GooF = 1.033. The *y* coordinate of one carbon atom of the host was fixed to define the origin in the structure CABN and polar axis restraints after Flack and Schwarzenbach[24] applied to define the origin in the structure CAPNOT.

All non-hydrogen atoms of the host molecules were refined anisotropically and methine, methylene and methyl hydrogen atoms were placed in geometrically generated positions and refined with positional parameters riding on the host atom with each type tied to a common temperature factor. Host hydroxyl hydrogen atoms for CAPNOT were located in difference electron density maps and refined with bond length restraints. All guest non-hydrogen atoms of CABN and the nitro group of *p*-nitrotoluene were refined isotropically with hydrogen atoms included at calculated positions as for the host molecules. Guest molecules were refined with site occupancy factors of unity based on the results of thermal analysis measurements.

Final fractional atomic coordinates, temperature factors, bond lengths and angles and tables of structure factors have been deposited at the Cambridge Crystallographic Data Centre.

Thermal Analysis

Differential Scanning Calorimetry (DSC) and Thermal Gravimetry (TG) were performed on a Perkin Elmer PC7 system.

Rising temperature thermal analysis: Crystals of the inclusion compounds were removed from mother liquor, blotted dry and lightly crushed before analysis. Sample masses in the range 1–5 mg were analysed in the temperature range 30–230 °C at a heating rate of 20 °C.min^{-1} with dry nitrogen purge gas at a flow rate of 40 cm^3.min^{-1}.

Isothermal thermogravimetry: Crystals of the inclusion compounds were grown as for X-ray diffractometry, filtered from the mother liquor, washed with dry diethyl ether, crushed and sieved. The fractions with particle sizes 212–250 μm and 63–125 μm were retained and the powders kept under an atmosphere of the relevant guest to prevent desorption of the guest. The desorption reactions were carried out under isothermal thermogravimetric conditions at temperatures in the ranges indicated in Table II. Resultant weight loss percentage *versus* time curves were converted to extent of reaction (α) *versus* time curves which were fitted to one of the common rate law equations.[25] The best fit was deemed to be that which most nearly approached linearity over the largest α range. Val-

TABLE II Thermal analysis data for all CA inclusion compounds included in the kinetic study.

	Guest	TG weight loss %		DSC
		calc.	exp.	T_{onset} (°C)
CAAN	Aniline	18.6	18.5	142
CAPNOT	*p*-Nitrotoluene	25.1	23.9	133
CABN	Benzonitrile	20.0	20.0	144
CANI	Nitrobenzene	23.2	22.9	160
CAPTOL	*p*-Toluidine	20.8	19.3	146

ues of the rate constant, k, thus obtained were used to produce Arrhenius plots for estimation of the activation energies.

X-ray diffraction: Powder diffraction spectra of the inclusion compounds and of the desolvated material were recorded at 294 K using the continuous scan mode and Cu-K_α radiation. Crystalline samples were crushed and the spectrum recorded over the 2θ range 6–36°. Calculated spectra were produced from crystal structure data using the program LAZYPULVERIX[26] modified to produce gaussian curves instead of lines.

RESULTS

Molecular numbering for each compound is illustrated in Figures 1 a and b. Host numbering follows conventional steroid numbering. The side chain conformation is puckered as defined by the torsion angle C(17)-C(20)-C(22)-C(23); 59.0(10)° and 54.7(9)° for CABN and CAPNOT respectively and both structures reveal the occurrence of steroid bilayers held together by host-host hydrogen bonding: O(28)-H(28O)O(29)-H(29O)O(25)-H(25O)O(26)-H(26O)O(27)-H(27O). The bilayers, puckered due to the curved nature of the host molecules, pack together leaving channels into which the guest molecules are packed in columns parallel to b. Host bond lengths and angles are similar to those found in related structures and guest geometry is reasonable.

The packing diagrams of CABN and CAPNOT are presented in Figure 2 a and b. Both exhibit the A-type packing mode[10] in which the C(18) methyl groups are in close contact about the screw diad at (0,y,1/2). The polar functional groups of the guests are oriented away from the channel walls and no short range host-guest interactions occur. The structures elucidated here are similar to those of the other aromatic guest inclusion compounds included in the kinetic study.

The host:guest ratios of all compounds used in the study were confirmed by weight loss percent on TG analysis. Rising temperature thermal analysis of these compounds indicates a single guest loss event evidenced by a single endotherm on DSC analysis and a single smooth weight loss on TG analysis. Calculated and experimental weight loss data and onset temperatures of guest loss are presented in Table II. Guest molecule site occupancy factors were fixed at unity as measured weight loss percent values on TG analysis agreed well with values calculated assuming 1:1 host:guest stoichiometry. It is possible that guest "holes" exist but it was deemed unwise to attempt refinement of guest site occupancy factors based on data collected at 21°C due to the relatively high thermal displacement parameters exhibited by the guest molecules. XRD analysis of the material remaining after complete desorption of the guest species from the various inclusion compounds confirms that a common polymorph of CA results.

Decomposition of this group of compounds resulted in sigmoidal α *versus* time curves which are best described by either an A2 (Avrami-Erofe'ev) or B1 (Prout-Tompkins) rate law; $kt = [-\ln(1-\alpha)]^{1/2}$ and $kt = \ln[\alpha/(1-\alpha)]$ respectively. Careful consideration of the range of temperatures over which each model applies and comparison of experimental curves and those regenerated from each model led to the selection of the B1 rate law as the better descriptor of the decomposition reactions of the aromatic guest inclusion compounds of CA although the estimated values of the activation energy of decomposition are similar in each case as is evident from consideration of the slopes of the lines in Figure 3a.

Values of k and the α ranges over which they apply are detailed in Table III and the Arrhenius plots resulting presented as Figure 3 a to e. The straight line nature of the plots confirms the isokinetic nature of the decomposition reactions

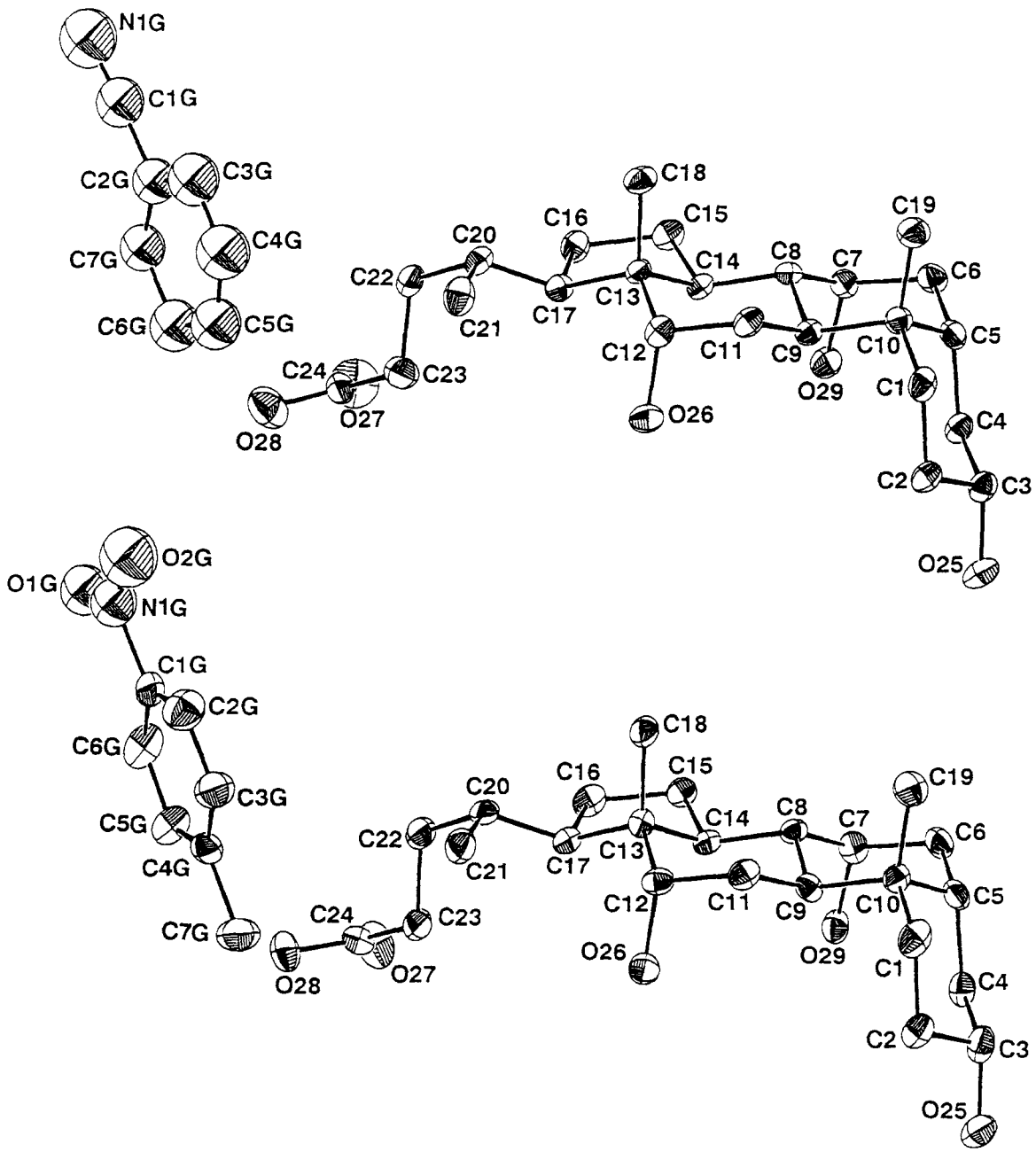

FIGURE 1 ORTEP plots at 30% probability for a) CABN and b) CAPNOT.

over the temperature range studied and values for Ea and *ln* A so derived are presented in Table IV. Interestingly the Arrhenius plot for CAPNOT shows the existence of two distinct lines with quite different slopes intersecting at a temperature of *ca* 116°C. This was initially puzzling as the fit of the α *versus* time curves to the B1 rate law was good over the entire temperature range.

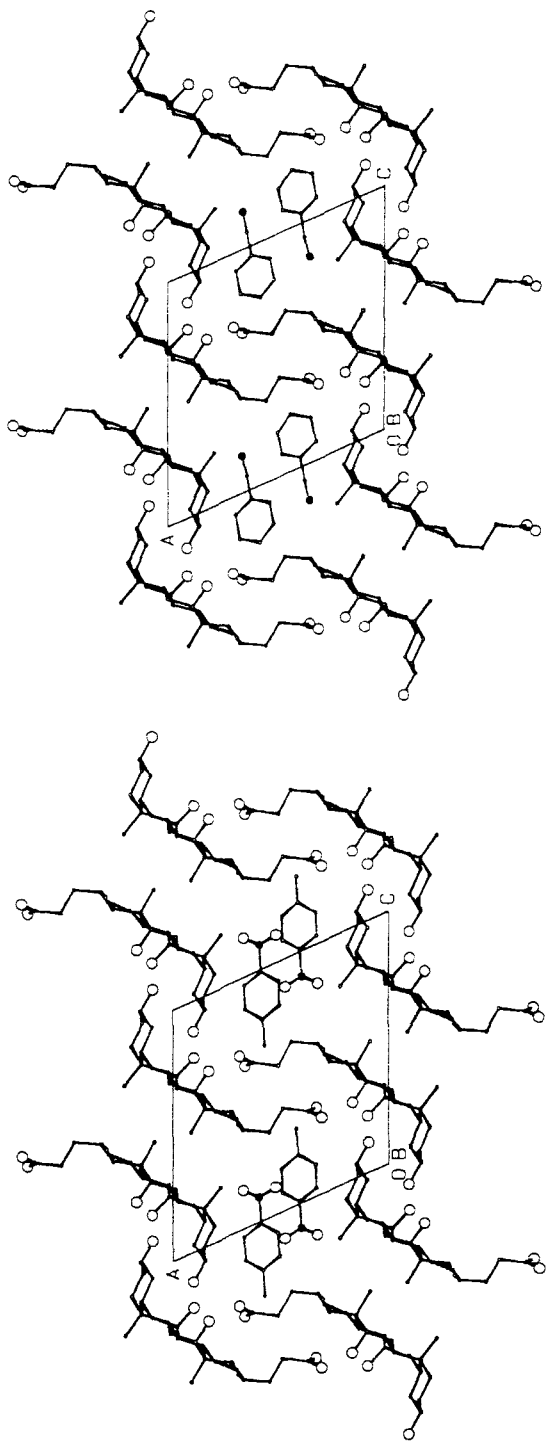

FIGURE 2 Packing diagrams viewed down [010] for a) CABN and b) CAPNOT.

Microscopic observation under heating and nitrogen flow indicates that above 116°C the crystallites undergo partial melting during decomposition. It is, of course, impossible to describe the mechanism of decomposition when partial melting occurs unless one is able to distinguish between vapour evolved from the melt and vapour evolved from the solid and this is not achieved when the rate of reaction is followed by measurement of a bulk property such as weight loss. However, it is interesting to note that the activation energy derived for decomposition with melting is significantly greater than without. While a number of other compounds were observed to undergo partial or complete melting concomitant with guest release on rising temperature thermal analysis the temperature range for decomposition was carefully chosen to ensure that the reaction monitored was the loss of gaseous guest from the *crystalline* complex rather than from the *melt* containing both host and guest.

Both the A2 and B1 rate laws are derived to account for mechanisms dominated by growth of nuclei of the product phase[27,28] implying that the formation of the new phase, CA(α), is the rate determining step. The derivation of either of these rate laws begins with the assumption that germ nuclei are already present and randomly distributed throughout the reactant phase and the B1 rate law is derived for branching growth of regions of the new phase[18]. The implication is that for decay to occur the molecule or molecular aggregate must be adjacent to either a product molecule or germ nucleus. The density of germ nuclei (or crystal defects) in the reactant crystal will therefore have a direct effect on the measured rate of reaction throughout the time period of the reaction as a greater number of growing nuclei implies more rapid conversion to product and shorter path lengths for growing branches before intersection and termination of growth as occurs in the deceleratory phase. The effect of increased defect density was qualitatively investigated by considering the effect of

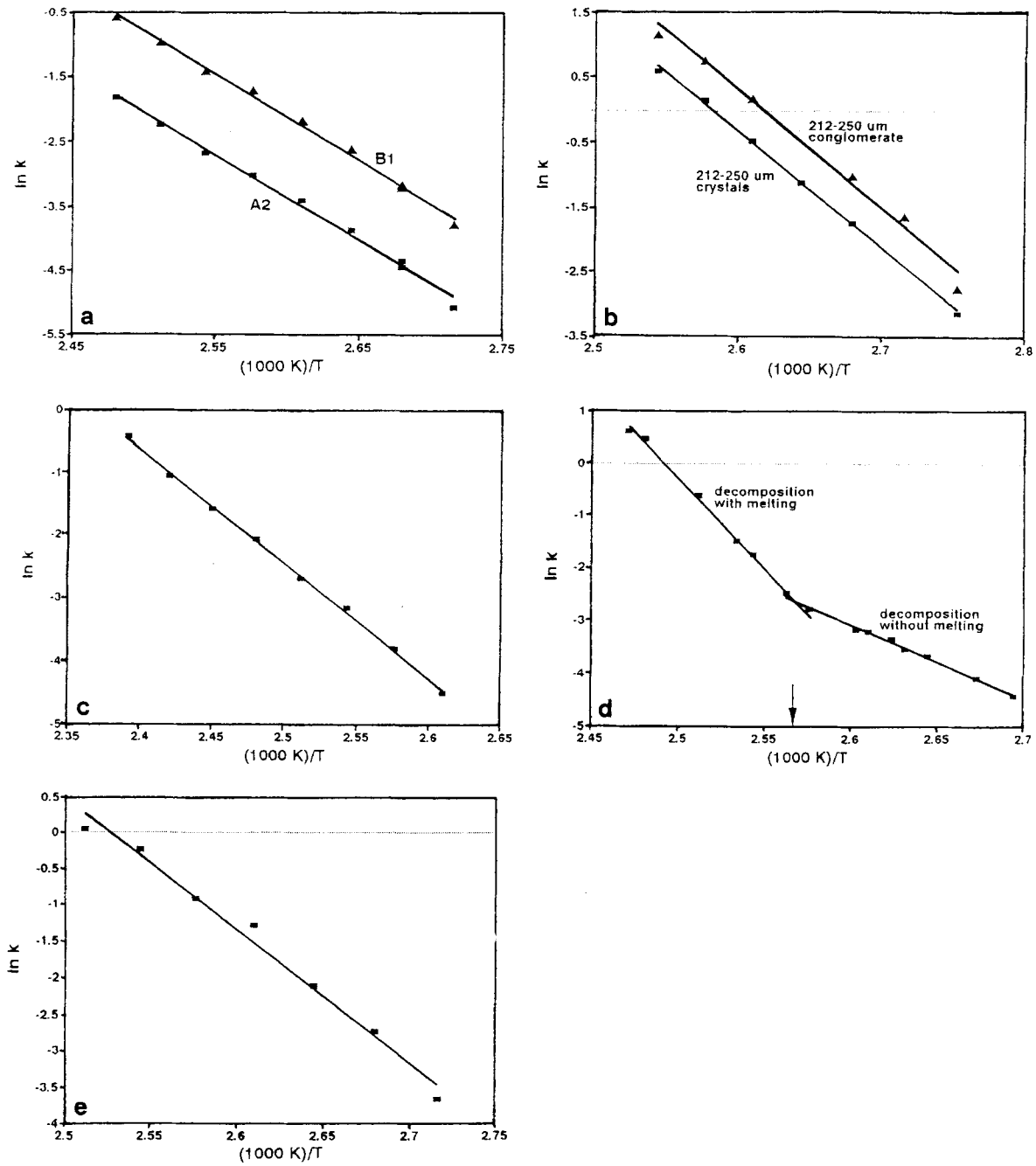

FIGURE 3 Arrhenius plots for a) CABN, b) CAAN, c) CANI, d) CAPNOT and e) CAPTOL.

TABLE III Analysis of decomposition isotherms for CA inclusion compounds with aromatic guests.

T(°C)	α-range	k (min^{-1})	r
CAAN (212–250 μm crystals)			
90	0.1 –0.85	0.0455(1)	0.997
100	0.1 –0.85	0.1735(5)	0.995
105	0.1 –0.95	0.328(2)	0.994
110	0.1 –0.95	0.626(2)	0.999
115	0.12 –0.95	1.160(2)	0.999
120	0.1 –0.95	1.80(1)	0.998
125	0.1 –0.95	2.35(2)	0.996
CAAN (212–250 μm conglomerate)			
90	0.15 –0.95	0.06427(4)	0.997
95	0.1 –0.95	0.1946(6)	0.999
100	0.1 –0.95	0.3621(3)	1.000
110	0.1 –0.95	1.222(9)	0.996
	0.1 –0.95	1.192(4)	0.999
115	0.1 –0.95	2.10(2)	0.996
120	0.1 –0.95	3.14(4)	0.994
CAPNOT (212–250 μm crystals)			
98	0.05 –0.95	0.00120(6)	0.982
101	0.10 –0.95	0.0170(1)	0.980
105	0.15 –0.95	0.0257(2)	0.989
107	0.05 –0.90	0.291(3)	0.978
108	0.10 –0.90	0.0353(4)	0.977
110	0.15 –0.95	0.0406(3)	0.983
111	0.24 –0.95	0.0422(4)	0.966
115	0.15 –0.95	0.0621(8)	0.989
117	0.2 –0.95	0.0941(4)	0.982
120	0.15 –0.95	0.172(2)	0.973
122	0.10 –0.95	0.237(2)	0.977
125	0.05 –0.95	0.537(7)	0.968
130	0.05 –0.95	1.58(1)	0.997
132	0.05 –0.95	1.838(8)	0.999
CABN (212–250 μm crystals)			
B1 95	0.1 –0.8	0.228(2)	0.994
100	0.1 –0.8	0.0426(6)	0.986
	0.1 –0.9	0.0409(4)	0.984
105	0.07 –0.9	0.0734(6)	0.991
110	0.07 –0.9	0.1142(9)	0.989
115	0.05 –0.9	0.181(2)	0.989
120	0.07 –0.95	0.242(2)	0.996
125	0.08 –0.95	0.376(1)	0.997
130	0.1 –0.95	0.552(4)	0.998
A2 95	0.1 –0.8	0.00623(2)	0.999
100	0.08 –0.8	0.01183(7)	0.997
	0.1 –0.85	0.01304(4)	0.999
105	0.1 –0.9	0.02088(7)	0.999
110	0.1 –0.85	0.03343(7)	0.999
115	0.05 –0.9	0.0491(2)	0.998
120	0.1 –0.95	0.0691(4)	0.998
125	0.15 –0.95	0.1075(1)	1.000
130	0.2 –0.95	0.1625(9)	0.999